Electric-field gradient in muscovites

LAURENCE P. ALDRIDGE, JAMES FINCH, A. ROSS GAINSFORD, W. CRAIGHEAD TENNANT

Chemistry Division, Department of Scientific and Industrial Research, Private Bag, Petone, New Zealand

CYRIL W. CHILDS

New Zealand Soil Bureau, Department of Scientific and Industrial Research, Private Bag, Lower Hutt, New Zealand

ABSTRACT

Single-crystal Mössbauer studies, supplemented by polarized optical-absorption measurements, were used to determine the EFG alignments of Fe^{2+} in the M1 and M2 sites and Fe^{3+} in the M1 site of three muscovites of varying Fe composition and color type. The EFG alignments differ markedly in the three crystals. In conformity with the requirements of crystal symmetry, but contrary to earlier reported results, the EFG symmetries are distinctly rhombic: $\eta = 0.68$, 0.70, and 0.93 for Fe^{2+}_{M1}, Fe^{2+}_{M2}, and Fe^{3+}_{M1}, respectively. There is a strong tendency for either $V_{\hat{y}\hat{y}}$ or $V_{\hat{z}\hat{z}}$ to align along an M1–M2 (or M1–M1) direction, particularly in a high Fe^{2+} (red-colored) muscovite.

INTRODUCTION

In an earlier paper (Finch et al., 1982) we examined the relations between polarized optical absorption and the distribution of Fe^{2+} and Fe^{3+} in the M1 and M2 sites in the octahedral layer of a series of $2M_1$ muscovites of widely differing color types and Fe compositions. The observed correlations led us to suspect that it might be meaningful to study the electric-field gradient (EFG) alignments of $Fe^{2+}_{M1,M2}$ and Fe^{3+}_{M1} in muscovites of a few typical color types. In particular we address the proposition that EFG alignment might be related, as are certain bands in the visible absorption spectrum, to the relative concentrations of Fe^{2+} and Fe^{3+} in adjacent edge-sharing M1–M1 or M1–M2 octahedra. A few preliminary Mössbauer measurements indicated that the relative intensities of the quadrupole doublets of $Fe^{2+}_{M1,M2}$ and Fe^{3+}_{M1} were markedly different in a typical "red" and a typical "green" muscovite.

Single-crystal Mössbauer measurements in sheet micas have a number of compensating advantages and difficulties. The sheet nature of the mineral with the crystal **a** and **b** axes in the basal plane means that large, thin, easily aligned crystals are readily obtainable in which the "thin-crystal limit" may be assumed as a reasonable approximation. Measurements in a single plane ($\gamma \perp \mathbf{b}$) produce most of the information necessary to obtain the EFG. The disadvantage is that because the Laue symmetry of the M1 and M2 sites is only $\bar{1}$ ($\equiv C_i$) in a monoclinic crystal, there is always an infinity of solutions in the absence of use of polarized radiation (Zimmerman, 1975; Gibb, 1978). This arises because one is measuring, in general, a macroscopic property (Zimmerman, 1975) of two symmetry-related sites in the monoclinic unit cell. As is usual in single-crystal Mössbauer studies, where more than one symmetry-related resonant center is present, the relative intensities of the lower- and higher-ve-

locity resonances of quadrupole split doublets are affected by both the transition probabilities of the nuclear transitions, calculable in the thin-crystal limit, and anisotropy in the recoil-free fraction, defined by the mean square displacement (MSD) tensor. Each of these quantities is determined as a second-rank tensor and, in the monoclinic case, the two tensors generally have noncoaxial principal directions (Grant et al., 1969).

In this study we report single-crystal Mössbauer measurements on three muscovites of the $2M_1$ polymorph which were chosen, on the basis of polarized optical absorption in the visible spectrum, as described earlier (Finch et al., 1982), to be typical of three color types: blue-green, brown-green, and red. Chemical analysis and Mössbauer measurements, on the samples as powders, confirmed the expected distribution of Fe as Fe^{2+} and Fe^{3+} in the M1 and M2 sites. In particular, the end-member red and green samples are typically high in Fe^{2+} and Fe^{3+}, respectively (Finch et al., 1982).

EXPERIMENTAL DETAILS

Description of samples

The three muscovites studied were taken from the Australian Harts Range collection described previously by one of us (Finch, 1963). Material was selected from large sheets in order to be well clear of any discernible color changes, inclusions, and imperfections. Plates, up to 0.5 mm thick, were cut with 20–50-mm edges parallel to the **a** and **b** crystallographic axes for absorption spectra. Single-crystal Mössbauer studies used crystals about 0.3 mm thick. Material for composition determinations and powder Mössbauer studies consisted of flakes cleaved from these plates and their immediate surroundings.

Chemical composition

Compositions were obtained by XRF analysis of fusion buttons prepared from flake material oven dried at 105°C. These analyses are shown in Table 1.

TABLE 1. Muscovite compositions* and colors

Color	BG4 blue-green	BH brown-green	RX red
SiO_2	45.84	45.92	45.65
Al_2O_3	31.68	30.10	33.86
K_2O	10.76	10.61	10.33
Na_2O	0.46	<0.30	1.38
CaO	0.10	<0.01	0.07
Fe_2O_3**	4.50	5.81	1.40
FeO**	1.40	1.37	1.32
TiO_2	0.18	0.40	0.37
Mn_2O_3	0.11	0.10	<0.03
MgO	0.52	1.48	1.34
H_2O†	4.62	4.30	4.68
Total‡	100.17	100.09	100.40

* Analytical results determined by XRF.
** Distribution of Fe as Fe^{2+} and Fe^{3+} from Mössbauer parameters.
† Determined as loss on ignition at 1000°C during sample preparation for XRF analyses.
‡ V and Cr contents were less than 0.01%.

Polarized absorption spectra

Absorption spectra for each of the Y and Z vibration directions were determined on an HP 845 diode-array recording spectrophotometer in which the exit beam was polarized with a Polaroid sheet placed between the exit window and the muscovite specimen and oriented perpendicular to the light beam. The instrument was programmed to produce absorption curves: (1) corrected for reflection loss (using a thin glass sheet as reference), (2) corrected to a standard thickness of 0.381 mm, and (3) finally plotted as log absorbance against linear wavelength to give $\lambda -$ log A curves. These latter allowed direct and simple comparisons of absorption features.

Mössbauer measurements

Mössbauer results were collected on two spectrometers: a Cryophysics microprocessor-based spectrometer, and an Elscint spectrometer, each operated in the constant acceleration (linear velocity response) mode. The source was 10 mCi $^{57}Co/Rh$, and the velocity and isomer-shift reference was the spectrum of soft Fe foil. Each spectrum was best-fitted to three pairs of overlapping Lorentzian lines using a least-squares program developed by one of us (Aldridge, 1984). Peak widths, for a given quadrupole doublet, were constrained to be equal, but all other constraints were relaxed.

Muscovite is monoclinic, space group $C2/c$, but the M1 and M2 sites have only $\bar{1}$ Laue symmetry; hence, there are, in fact, two symmetry-related resonant sites (for the Mössbauer nucleus in each of M1, M2) per unit cell (Gibb, 1978). In the plane perpendicular to the twofold axis, **b** (i.e., the **a**-**c** plane), the two resonant sites, related by 180° rotation about **b**, are equivalent. Initially, therefore, data was collected in 15° steps in this plane using the reference coordinates defined in Figure 1. Here γ is a unit vector—$[\sin\theta\cos\phi, \sin\theta\sin\phi, \cos\theta]$ referred to an orthogonal coordinate system $[x, y, z] = [c^*, a, b]$—along which the gamma beam is directed.

From the fitted-peak areas we obtained relative intensities $I^{(h)}$ and $I^{(l)}$ and reduced intensities $I^{(r)} = I^{(h)}/(I^{(h)} + I^{(l)})$, where $I^{(h)}$ and $I^{(l)}$ are the high and low relative intensities of each of the quadrupole doublets. Generally the peaks of Fe^{2+}_{M1}, Fe^{3+}_{M1} predominate, and their relative intensities are well determined; Fe^{2+}_{M2} peaks on the other hand make only a small contribution to the total area
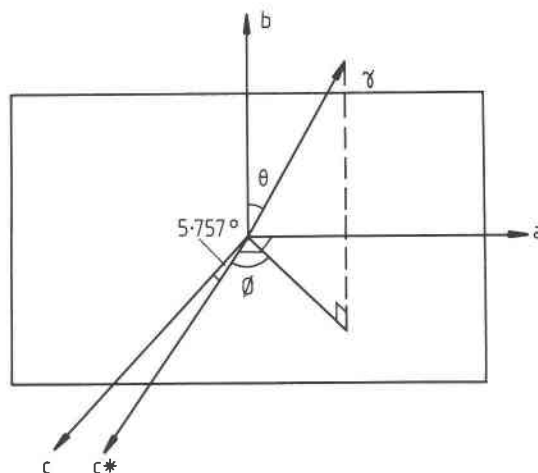

Fig. 1. The coordinate system used, in relation to the crystal axes **a**, **b**, and **c**. γ is an arbitrary unit vector with polar angle θ and azimuthal angle ϕ.

and are generally poorly determined. Now each of $I^{(r)}$, $I^{(h)}$, and $I^{(l)}$ behaves, ideally, as a second-rank tensor quantity and therefore is expected to follow the relation

$$I = A + B\cos 2\phi + C\sin 2\phi \qquad (1)$$

(Weil et al., 1973). We used least-squares to fit $I^{(h)}$, $I^{(l)}$ for Fe^{2+}_{M1}, Fe^{3+}_{M1} to Equation 1, eliminating "rogues" thereby, and used similar plots of Fe^{2+}_{M2} and the necessary condition $I^{(total)} = 1$ to obtain the weak relative intensities of the Fe^{2+}_{M2} peaks. Intensity data reported in the following section have been idealized in this way.

RESULTS

Table 1 identifies the three muscovites studied and details their compositions as obtained by XRF. Figure 2 shows the polarized absorption spectra in the region 4000–7000 Å. ^{57}Fe Mössbauer results for the three powdered samples
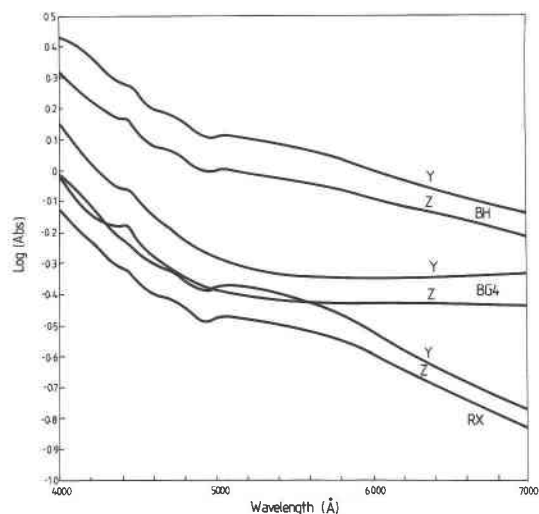

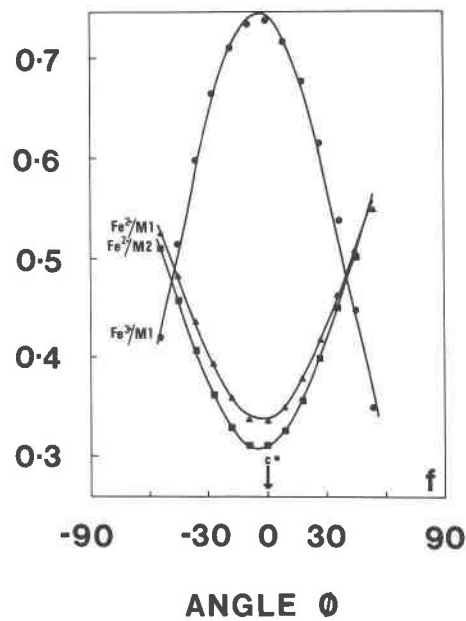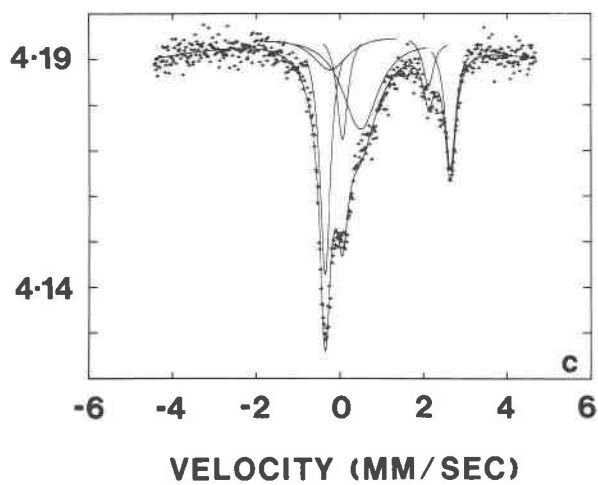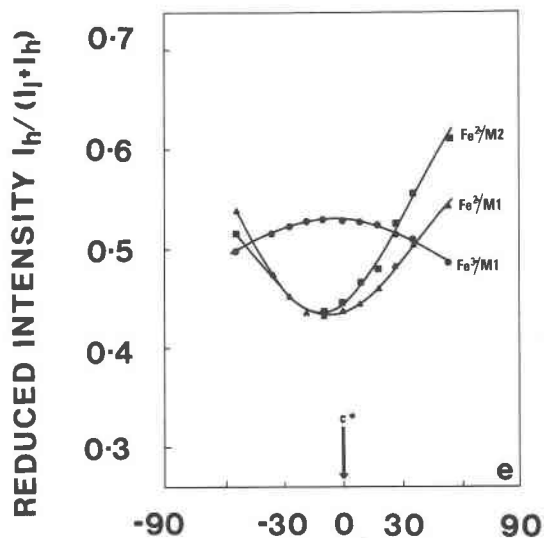Fig. 2. Optical-absorption spectra in the two principal vibration directions in the basal plane.
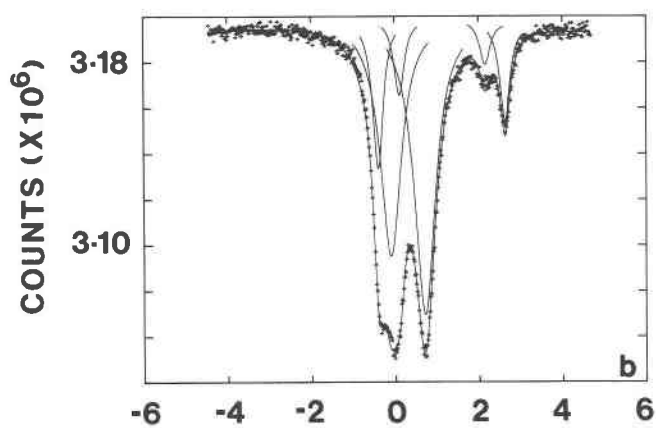
a:Fe²⁺/M1
b:Fe²⁺/M2
c:Fe³⁺/M1
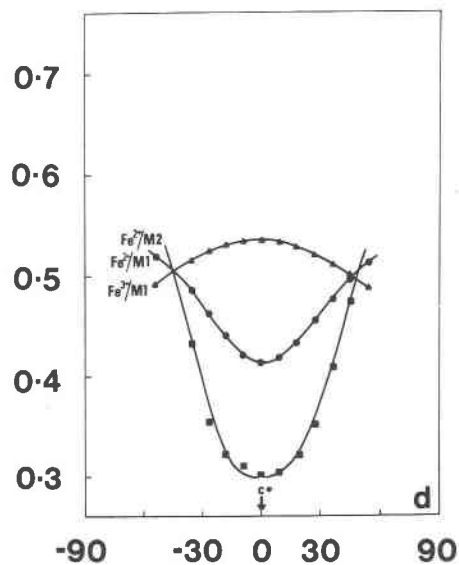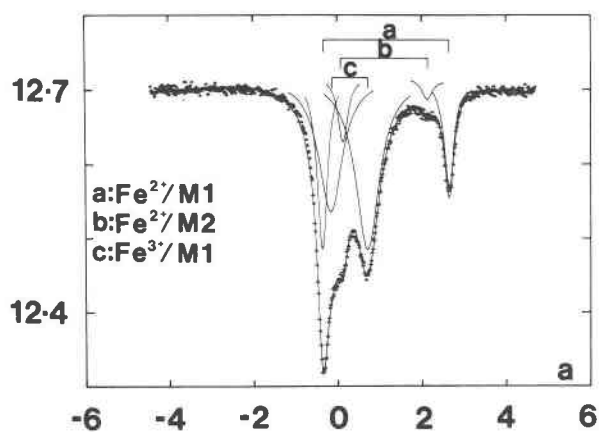
TABLE 2. Distribution of Fe^{2+} and Fe^{3+} and Mössbauer parameters of the three muscovites

	Total Fe (%)	Fe^{2+}_{M1}				Fe^{2+}_{M2}				Fe^{3+}_{M1}			
		%	I.S.	Q.S.	L.W.	%	I.S.	Q.S.	L.W.	%	I.S.	Q.S.	L.W.
BG4	4.24	18.2	1.09	2.98	0.349	7.5	1.02	2.09	0.458	74.3	0.32	0.83	0.805
BH	5.13	12.9	1.08	2.99	0.482	7.8	1.09	2.11	0.315	79.3	0.33	0.90	0.706
RX	2.01	30.3	1.10	2.97	0.348	20.8	1.09	2.05	0.435	48.9	0.32	0.88	0.736

Note: Columns as follows: % = percent of total Fe; I.S. = isomer shift (mm/s) relative to Fe metal; Q.S. = quadrupole splitting (mm/s); L.W. = line width (FWHM, mm/s).

are listed in Table 2. Single-crystal Mössbauer spectra of each of the crystals observed with the gamma beam directed along c^* (refer to Fig. 1) are shown in Figures 3a–3c. The measured angular variation of reduced intensity in the a–c-plane for each of the crystals is shown in Figures 3d–3f.

DISCUSSION

Derivation of the EFG tensor

In pioneering papers, Zory (1965) and Zimmerman (1975) showed that the traceless second-rank EFG tensor, $\bar{V}$, is equivalent to a traceless reduced intensity matrix, hereafter designated $\bar{I}$. The elements of the traceless tensor $\bar{I}$ and the experimental "tensor" $\bar{I}^{(r)}$ are related by $I_{pq} = I^{(r)}_{pq} - \frac{1}{2}\delta_{pq}$ ($\delta_{pq} = 0$, $p \neq q$ and $\delta_{pq} = 1$, $p = q$). The traceless tensors $\bar{V}$ and $\bar{I}$ are proportional and diagonal in the same principal axis system. With polar angle θ and azimuthal angle ϕ defined as in Figure 1, the reduced intensities $I_{\pm}$ for the two symmetry-related resonant species have the following angular dependence:

$$I_{\pm} = I_{xx}\sin^2\theta\,\cos^2\phi + I_{yy}\sin^2\theta\,\sin^2\phi$$
$$+ I_{zz}\cos^2\theta + I_{xy}\sin^2\theta\,\sin 2\phi$$
$$\pm I_{xz}\sin 2\theta\,\cos\phi \pm I_{yz}\sin 2\theta\,\sin\phi \quad (2)$$

(Weil et al., 1973). In the plane perpendicular to **b**, i.e., $\theta = 90°$ (refer to Fig. 1) the two reduced intensities are degenerate. Rotations in the plane perpendicular to **b** (the data illustrated in Figs. 3d–3f) yield the elements I_{xx}, I_{yy}, and I_{xy} and, from the zero trace condition, I_{zz}. Further, invariance of the square of the "length" of the vector $[(\sqrt{3}/2)I_{zz}, \frac{1}{2}(I_{xx} - I_{yy}), I_{xy}, I_{xz}, I_{yz}]$ under coordinate rotation (McGavin and Tennant, 1985a), yields $I^2_{xz} + I^2_{yz}$ (Zimmerman, 1975).

From Table 2 it can be seen that the quadrupole splitting (Q.S. or ΔE_Q) and isomer shift (I.S.) for Fe^{2+}_{M1}, Fe^{2+}_{M2}, and Fe^{3+}_{M1} are very similar in the three muscovites under study. The quadrupole splitting is given by the relation

$$\Delta E_Q = \frac{1}{2}eQV_{\hat{z}\hat{z}}(1 + \eta/3), \quad (3)$$

where $\eta = (V_{\hat{x}\hat{x}} - V_{\hat{y}\hat{y}})/V_{\hat{z}\hat{z}}$ is the asymmetry parameter

and $V_{\hat{x}\hat{x}}$, $V_{\hat{y}\hat{y}}$, and $V_{\hat{z}\hat{z}}$ are the principal values of the EFG tensor ($|V_{\hat{z}\hat{z}}| \geq |V_{\hat{y}\hat{y}}| \geq |V_{\hat{x}\hat{x}}|$), e is the electronic charge, and Q is the quadrupole moment of the ^{57}Fe excited state. Equation 3 and the quadrupole-splitting data of Table 2 indicate that the principal values of the EFG tensor in the three muscovites are identical, within the limits of experimental error, for each of the quadrupole doublets. It then seems reasonable to assume, since the crystals are of approximately equal thickness (ca. 0.3 mm), and the MSD tensor is not expected to be markedly different, that the very different reduced intensity plots of Figures 3d–3f must arise from differently aligned EFG tensors in the three crystals. [The thickness effect is better treated as an effective thickness expressed as quantity of absorbing species per unit of area. That the neglect of thickness is a reasonable assumption was checked for the RX muscovite by stacking several layers (total thickness 1.6 mm) and determining the Mössbauer intensity ratios for $\gamma \perp$ c^*. Extrapolation to zero thickness indicated negligible (<5%) errors in any of the intensity ratios in assuming zero thickness for our crystal (actual thickness 0.25 mm or, 1.4 mg/cm² total Fe).] Therefore, we sought matrices, $\bar{I}$, corresponding to each quadrupole doublet, with equal eigenvalues, but different eigenvectors. This was achieved by varying I_{xz} and I_{yz} within the constraint $I^2_{xz} + I^2_{yz} =$ constant, numerically diagonalizing the intensity matrices and plotting the quantity $I_{\hat{x}\hat{x}} \times I_{\hat{y}\hat{y}} \times I_{\hat{z}\hat{z}}$ vs. $I^2_{xz}/(I^2_{xz} + I^2_{yz})$ for each center in each muscovite. In principal, a "triple point" exists from which we obtain I_{xz} and I_{yz} and the eigenvectors of the diagonalized intensity matrices. In practice, exact coincidence was never quite realized, and the mean of three crossovers was taken. Thus in the approximations—(1) thin-crystal limit, (2) neglect of polarization effects, and (3) neglect of effects from the MSD tensor—the alignment of the principal values of the I matrix and hence the EFG tensor can be found. These are listed in Table 3. In each case there is a symmetry-related EFG tensor, demanded by $C2$ crystal point-group symmetry, obtained by rotating the tensor principal directions 180° about **b**. This has the effect of taking the azimuthal angle ϕ into $\phi + 180°$. The principal directions

←

Fig. 3. Single-crystal Mössbauer spectra ($\gamma \perp c^*$) and measured angular variation of reduced intensity in the a-c plane. (a) and (d), BG4; (b) and (e), BH; (c) and (f), RX.

TABLE 3. Principal values and directions of EFG tensors

BG4 muscovite				BH muscovite				RX muscovite			
$\bar{I}$ principal value	Principal directions			$\bar{I}$ principal value	Principal directions			$\bar{I}$ principal value	Principal directions		
	θ	ϕ_1	ϕ_2		θ	ϕ_1	ϕ_2		θ	ϕ_1	ϕ_2
Fe^{2+}_{M1}											
0.232(2)	130.3	252.4	72.4	0.233(2)	128.5	250.5	70.5	0.233(2)	122.7	260.6	80.6
−0.036(5)	109.8	144.6	324.6	−0.038(6)	106.9	146.6	326.6	−0.037(5)	42.8	306.7	126.7
−0.196(3)	46.9	215.0	35.0	−0.195(3)	43.3	217.8	37.8	−0.196(3)	65.7	187.4	7.4
$\eta = 0.693(30)$				$\eta = 0.676(40)$				$\eta = 0.682(35)$			
Fe^{2+}_{M2}											
0.197(3)	112.7	273.1	93.1	0.197(3)	113.2	277.7	97.7	0.197(3)	120.6	275.1	95.1
0.035(5)	27.8	235.4	55.4	0.035(5)	60.0	202.2	22.2	0.035(5)	38.9	232.3	52.3
−0.232(2)	74.8	356.5	176.5	−0.232(2)	39.7	336.3	156.3	−0.232(2)	68.4	351.6	171.6
$\eta = 0.698(40)$				$\eta = 0.700(40)$				$\eta = 0.699(40)$			
Fe^{3+}_{M1}											
0.220(1)	133.4	329.6	149.6	0.220(1)	133.6	327.7	147.7	0.220(1)	95.7	356.8	176.8
−0.007(2)	99.0	231.0	51.0	−0.008(1)	96.9	231.0	51.0	−0.007(1)	7.3	35.6	215.6
−0.213(1)	44.8	311.8	131.8	−0.212(2)	44.4	313.9	133.9	−0.213(0)	85.5	267.3	87.3
$\eta = 0.933(20)$				$\eta = 0.931(20)$				$\eta = 0.933(20)$			

Note: Error estimates in parentheses; all angles in degrees. Angles θ and ϕ are as defined in Figure 1; ϕ_1 and ϕ_2 refer to sites 1 and 2, respectively (see text).

are then θ, ϕ and θ, ϕ + 180°, respectively, for species 1 and 2. As discussed later, only one of these need be considered explicitly.

General discussion

The polarized absorption spectra of Figure 2 typify the three color types of the muscovites chosen for study and have been discussed in detail elsewhere (Finch et al., 1982). The main features are, in summary, the intense absorption maximum that peaks in the ultraviolet and tails off into the visible between 4000–5000 Å (assigned to Fe^{2+}-ligand charge transfer), the sharp Fe^{3+} *d–d* transition ($^6A_1 \rightarrow {}^4A_1$, ^4E) at 4430 Å, and the broad maximum between 5000 and 6000 Å thought to arise from metal-metal charge transfer between Fe^{2+} and Fe^{3+} ions in adjacent edge-sharing M1–M1′ or M1–M2 octahedra. It is this latter feature that is of predominant interest in discussing the EFG alignments in the present study.

In the following discussion we have assumed, as earlier (Finch et al., 1982) and following Goodman (1976), that M1 is the normally occupied, smaller, more distorted site with *cis*-hydroxyls and M2 is the larger, normally unoccupied, less distorted site with *trans*-hydroxyls. We are aware, however, and accept that the alternative convention with *cis*-M2 and *trans*-M1 assignments is now likely to be adopted as the standard nomenclature for the octahedral sites (Dyar and Burns, 1986).

From Table 2 the Mössbauer spectral line widths (FWHM) in the powdered samples for Fe^{2+} (0.32–0.48 mm/s) are considerably greater than those typically observed for Fe^{2+} in minerals when single sites are assured (Bancroft, 1973). The Fe^{3+} line widths (0.7–0.8 mm/s) are very much greater than those observed for single sites, and even though the χ^2 values associated with fitting the spectra do not seem to justify it (Goodman, 1976; Finch et al., 1982), the suspicion that multiple sites could be

involved remains. In the absence of evidence to the contrary, we have ignored the possibility that some of the Fe^{3+} is present in tetrahedral sites. [However, see arguments by Richardson and Richardson (1982) and Annersten and Hålenius (1976) regarding tetrahedrally coordinated Fe in pink muscovite.] The single-crystal line widths showed a marked variation with crystal orientation. The line widths of Fe^{2+} range from 0.26 mm/s to 0.4 mm/s and have the same angular dependence as the reduced areas (refer to Figs. 3d–3f), that is, maximum widths where the variation of reduced area with angle is greatest and minimum widths at the turning points. Similar behavior has been observed in the electron paramagnetic resonance spectra of Fe^{3+} in α-quartz (Mombourquette et al., 1986) and in calcium tungstate (McGavin and Tennant, 1985b). In these examples and in the present instance, it seems likely that there is a distribution of spin-Hamiltonian parameters and that the measured parameters are in fact averages of ensembles giving rise to the observed variation of line width. We have suggested previously (Finch et al., 1982) that bands in the polarized absorption spectra near 5000 Å (e.g., see RX muscovite in Fig. 2) arise from $Fe^{2+} \rightarrow Fe^{3+}$ charge transfer. Bancroft (1973) has pointed out that the electric field produced by Fe^{2+} (or Fe^{3+}) in a site adjacent to Fe^{2+} would be expected to differ slightly, with consequent difference in ΔE_Q, from that produced by, say, Ca^{2+} or Mg^{2+}. There is also a further and more profound possibility, namely, that the alignment of the (average) EFG of the ensembles varies as the concentration of Fe^{2+} versus Fe^{3+} in adjacent edge-sharing octahedra varies. We discuss this further below.

The error estimates in $\bar{I}$ principal values and in η values given in Table 3 imply a precision in determining the $V_{\hat{x}\hat{x}}$, $V_{\hat{y}\hat{y}}$, and $V_{\hat{z}\hat{z}}$ alignments of 1° or 2°. In view of the approximations made, however, it is probable that the uncertainties are considerably greater than this. Before

discussing the detail of the EFG alignments, it is useful to make some general remarks regarding earlier work on muscovite and biotite single crystals and its relation to the requirements of crystal symmetry. From Figures 3d–3f the angular variation of $I^{(r)}$ has either a maximum or a minimum near the crystal **c** axis, i.e., approximately perpendicular to the basal plane of the crystal, which is the **c*** direction. In the case of one of the crystals, RX (Fig. 3f), the angular variation is large; for Fe^{3+}_{M1} in particular (see also Table 3), it is apparent that the plot is close to a principal plane of $\bar{V}$ ($\sim \bar{I}$). We examine two extreme possibilities:

(1) **Axial symmetry for** $\bar{V}$. $V_{\bar{z}\bar{z}}$ is taken to lie along **c*** and $\eta = 0$; the theoretical intensities in the ideal case with thin-crystal limit are $I^{(r)}_{\parallel} = 0.75$ and $I^{(r)}_{\perp} = 0.375$ (the corresponding values of the traceless intensity matrix $\bar{I}$ are $I_{\parallel} = 0.25$ and $I_{\perp} = -0.125$), and the quadrupole doublet is symmetrical ($I^{(r)} = 0.5$) when the gamma beam is at 54.7° to **c***.

(2) **"Complete rhombic" symmetry for** $\bar{V}$. $V_{\bar{z}\bar{z}} = -V_{\bar{y}\bar{y}}$, $\eta = 1$, and we let $V_{\bar{z}\bar{z}}$ lie along **c*** and $V_{\bar{y}\bar{y}}$ lie along **a**; the theoretical intensities in the **a**-**c*** plane are $I^{(r)}_{\bar{z}\bar{z}} = 0.716$ and $I^{(r)}_{\bar{y}\bar{y}} = 0.283$ (0.216 and -0.216, respectively, for the traceless matrix $\bar{I}$) and $I^{(r)} = 0.5$ when the gamma beam makes a 45° angle with **c***. With this choice of $\bar{V}$, all planes containing **c*** have symmetrical intensity plots about **c***, and one can always find a plane where $I^{(r)} \approx 0.5$ at about 55° to **c***.

Our present results for Fe^{3+}_{M1} (Fig. 3f) in the **a**-**c*** plane are more consistent with the complete rhombic case, but there are obviously an infinity of other possibilities. It would clearly be wrong to assume in the present instance, however, as has apparently been done for biotites (Chandra and Lokanathan, 1977; Ballet and Coey, 1982; Townsend and Longworth, 1985), that symmetrical quadrupole doublets at about 55° to **c*** (plane of measurement unspecified) indicate that $V_{\bar{z}\bar{z}}$ lies along **c*** and that the symmetry is axial ($\eta = 0$). Further, the results of these authors for biotites and a muscovite (see, in particular, Ballet and Coey, 1982) make it imperative to distinguish the axial and rhombic possibilities. As noted above, plots such as Figure 3f, assuming a principal plane, do not easily allow us to distinguish axial and complete rhombic symmetry; yet the latter is as far removed from axial symmetry as it is possible to be.

Muscovite crystallizes in the monoclinic space group $C2/c$, and no site in the crystal can have higher than monoclinic ($C2$) point-group symmetry; in fact, as already noted, the M1 and M2 sites have only triclinic symmetry [more correctly, because of the requirements of time-reversal invariance, an effective center of inversion is imposed upon the site and the (Laue) symmetry is $\bar{1}$ ($\equiv C_i$)]. Hence, the EFG tensor can only have orthorhombic symmetry although at the local level the symmetry may appear higher for some particular choice of reference coordinates. For muscovite Fe^{2+}_{M1}, two earlier studies reported axial symmetry (Ballet and Coey, 1982) and rhombic symmetry, $\eta = 0.6$–1.0 (Bonnin and Muller,

1981). No results have been reported for Fe^{2+}_{M2} or Fe^{3+}_{M1} to our knowledge. Electron paramagnetic resonance results for Fe^{3+} in micas have not been easy to fully interpret, but results reported for muscovite (Kemp, 1973) and phlogopite (Kemp, 1972) have in common strong, near-isotropic resonances near $g_{eff} = 4.3$, a condition that is almost invariably interpreted as arising from near-complete rhombicity in the second-degree fine-structure terms ($|E| \approx |D|/3$) for the Fe^{3+} site. Our present Mössbauer results indicate rhombic symmetry for the EFG tensors in conformity with the requirements of crystal symmetry.

The EFG alignment data of Table 3 is summarized in Figures 4a–4f, which depict the tensor alignments, for one of the symmetry-related species, with respect to the bounding M1 and M2 octahedra in a **c**-axis projection of the unit cell. Figures 4a–4f show only one of a number of possibilities. The M1 and M2 sites depicted are two adjacent sites in the unit cell, the origin being midway between the two *cis*-hydroxyls, OH(3) and OH(4). In each case we have shown the orientation of only one of the symmetry-related tensors (species 1), and, for example, Figure 4a shows only one of four ways of siting the EFGs for two Fe^{2+} ions. There are also four ways of siting the EFGs of Fe^{3+} and Fe^{2+} in the adjacent M1 and M2 sites, but for convenience of illustration (Figs. 4d–4f) we have only shown one Fe^{3+} EFG and left M2 unoccupied. The foregoing are unresolvable ambiguities but do not prevent us from drawing useful conclusions from our EFG data. For the three muscovites studied, in the sequence BG4 → BH → RX, the following gradation of properties is apparent: green → green-brown → red; decreasing concentration of Fe^{3+}; decreasing intensity of Fe^{3+} d–d transition at 4430 Å; increasing occupancy of M2 by Fe^{2+}; increasing intensity of broad absorption band, 5000–6000 Å; and increasing tendencies for $V_{\bar{z}\bar{z}}$ Fe^{2+}_{M1} to lie along the M1–M2 direction, for $V_{\bar{y}\bar{y}}$ Fe^{2+}_{M2} to lie along the M1–M2 direction, and for $V_{\bar{z}\bar{z}}$ Fe^{3+}_{M1} to lie along the **c*** direction. For convenience, therefore, we have ordered our tables and figures in the sequence BG4 → BH → RX.

We have noted previously the importance of Fe^{2+}_{M2} occupancy in determining the optical-absorption properties of muscovites. It is now apparent that Fe^{2+}_{M2} occupancy is crucially important to our understanding of the EFG alignments of $Fe^{2+}_{M1,M2}$ and Fe^{3+}_{M1}. More particularly, the relative concentrations of Fe^{2+} and Fe^{3+} in adjacent (edge-sharing) M1–M2 or M1–M1 octahedra is, as for optical properties, very important. For this reason the EFG alignments vary from sample to sample, and it is no longer sufficient to talk of EFG alignment in muscovite without first defining *which* muscovite.

Details of EFG alignment in relation to the muscovite unit-cell structure will now be considered for each Mössbauer center in turn. Since in all cases $|V_{\bar{x}\bar{x}}| \ll |V_{\bar{y}\bar{y}}|$ and $|V_{\bar{z}\bar{z}}|$, we shall only discuss $V_{\bar{y}\bar{y}}$ and $V_{\bar{z}\bar{z}}$ alignments. All crystallographic calculations are based on the X-ray data of Güven (1971).

(1) Fe^{3+}_{M1}. From the **c**-axis projections of Figure 4, the tendency for $V_{\bar{z}\bar{z}}$ for one of the symmetry-related EFGs
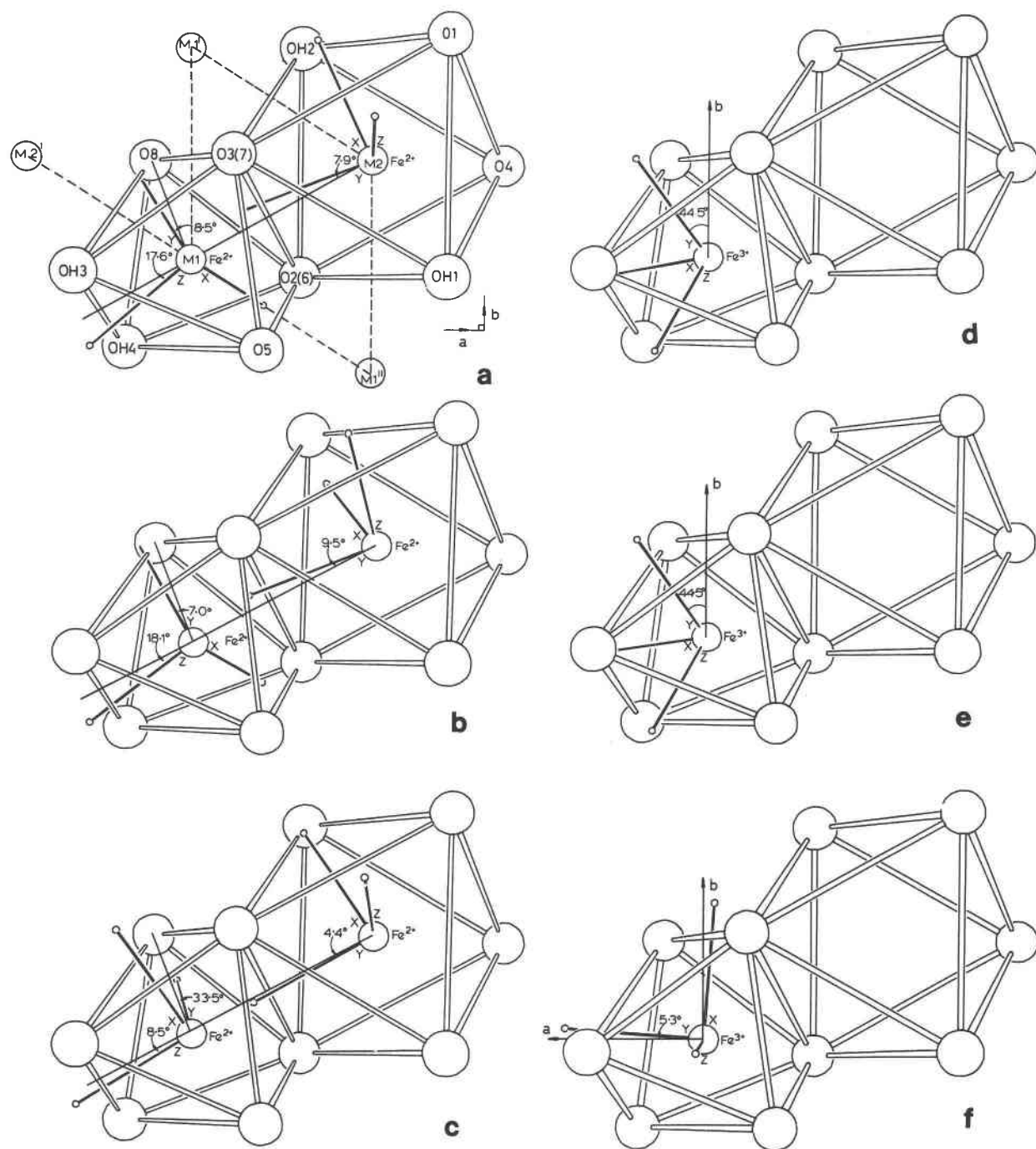
Fig. 4. The alignment of (a–c) Fe^{2+} and (d–f) Fe^{3+} EFGs with respect to the M1 and M2 octahedra: (a) and (d), BG4; (b) and (e), BH; (c) and (f), RX (see text for details).

to align along the M1–M2 direction is apparent, being closest for RX. The actual angles between $V_{\bar{z}\bar{z}}$ and M1–M2 are 17.6°, 18.1°, and 8.5° for BG4, BH, and RX, respectively. $V_{\bar{y}\bar{y}}$ lies close to the M1–O(8) [or M1–O(5)] direction in BG4 and BH, the angles being 8.5° and 7.0°, respectively. In RX the angle is 33.5°, $V_{\bar{y}\bar{y}}$ being directed toward the normal to the muscovite sheet; the angle with

c^* is about 26°. It is importnat to note that it is $V_{\bar{y}\bar{y}}$ and not $V_{\bar{z}\bar{z}}$ that is tending to align along c^* in RX and that the symmetry of $\bar{V}$ is far from axial. In fact, η is about 0.69 for Fe^{3+}_{M1} in all three crystals. The expectations of rhombic symmetry for $\bar{V}$ in a distorted site in a monoclinic crystal are realized.

It is convenient here to consider how the symmetry-

related EFGs for Fe^{2+} are oriented with respect to the M1 and M2 sites. We restrict the argument to the BG4 muscovite. Using the data of Table 3, for Fe^{2+}_{M1}, V_{zz} lies 17.6° away from the dashed line M1–M2′, and V_{yy} lies 8.9° from M1–O(7) (Fig. 4a), whereas for Fe^{2+}_{M2}, V_{yy} lies 7.9° away from the dashed line M1′–M2. These are the same relations that the first EFG has with the M1–M2 direction and that V_{yy} (Fe^{2+}_{M1}) has with M1–O(8). In general, if the EFG has some particular relation to an M1–M2 direction, or to a special direction in the bonding octahedron, then the symmetry-related EFG has the same relation to another M1–M2 direction or an equivalent special direction in the octahedron. Hereafter we shall only explicitly consider the alignment of EFG 1.

(2) Fe^{2+}_{M2}. Here it is V_{yy} that lies approximately along the M1–M2 direction, the angles being 7.9°, 9.5°, and 4.4° for BG4, BH, and RX, respectively. V_{zz} lies roughly in the plane containing the *trans*-hydroxyls, approximately perpendicular to the M1–M2 direction. The orientation of V_{zz} in this plane is markedly different in the three crystals. In BG4 and RX, V_{zz} lies near the c* axis at angles 15° and 22°, respectively, whereas for BH the angle is 54°. V_{zz} in BH in fact lies close (15° away) to the direction of the bisector of O(1)–M2–O(3). It is seen from Figure 4 that c* is very close (the angle is 0.25°) to a pseudo-three-fold direction in the M2 octahedron that might, in terms of local symmetry, suggest an approximation to trigonal symmetry. However, although V_{zz} in two of the crystals lies close to this direction, the η value of 0.70 indicates that the symmetry is far from axial. Our results seem to indicate that I_{zz} and, therefore, V_{zz} (Zimmerman, 1975) have different signs in M1 and M2, but we view this result with some suspicion and may have to review our position when theoretical calculations, now in progress (Aldridge et al., unpub.), become available.

(3) Fe^{3+}_{M1}. In this instance $\eta = 0.93$ in each crystal, and the symmetry of $\bar{V}$ approaches "complete rhombicity," i.e., $V_{zz} \approx -V_{yy}$, $V_{xx} \approx 0$. It is convenient then to discuss the EFG alignment in terms of planes that contain both V_{yy} and V_{zz} and their relation to the crystal axes. From Table 3 and Figure 4f, it is apparent that V_{zz} and V_{yy} lie approximately along c* and a, respectively, in the RX muscovite; the angles between these directions are 6.5° and 5.3°. In the BG4 and BH muscovites, on the other hand, the plane containing V_{yy} and V_{zz} lies approximately (within 10°) coincident with the plane defined by $\phi = 135°$ (Fig. 1). This plane also contains b, and V_{yy} and V_{zz} make angles of 44.5° and 133.6°, respectively, with b in both BG4 and BH. Thus, to a good approximation, the $\bar{V}$ principal values lie along the crystal axes in the "red" muscovite RX but lie well away from the axes in the two "green" muscovites BG4 and BH. In a low-symmetry site in a monoclinic crystal, there is no reason a priori to expect any crystallographic axis to be a special tensor direction. However, we have noted above that c* is close to a pseudo-threefold axis of the M1 (or M2) octahedron and that a also lies close (18° away) to a pseudo-threefold direction. In RX the plane containing V_{yy} and V_{zz} is ap-

proximately perpendicular to b (the V_{xx} direction), which is the line joining M1 to the midpoint of O(7)–O(8), i.e., to the midpoint of an M1 octahedron edge. This direction also defines the M1–M1′ direction for two edge-sharing M1 octahedra. Thus it appears that the $\bar{V}$ principal directions in the red muscovite, RX, which also has the lowest Fe^{3+} content and high occupancy of both M1 and M2 by Fe^{2+}, are closely related to special directions in the M1 octahedron. $\bar{V}$ principal directions in the two green muscovites, on the other hand, tend to "avoid" these special directions.

Our experiments indicate that the sign of V_{zz} for Fe^{3+}_{M1} is opposite to that for Fe^{2+}_{M1}. The absolute sign of V_{zz} is not known at this stage.

SUMMARY AND CONCLUSIONS

The focus of the present work is the markedly different single-crystal Mössbauer intensities that occur in muscovites of different color types. We have interpreted these results in terms of a model where the EFG for a given center has the same principal values but is aligned differently in different muscovites. The differences in alignment seem to arise from varying Fe^{2+} and Fe^{3+} concentrations in edge-sharing M1–M2 or M1–M1 octahedra. As a consequence of electron exchange between Fe^{2+} and Fe^{3+} in such pairs, V_{yy} or V_{zz} of the EFG tends to align along the M1–M2 direction. For Fe^{3+}_{M1}, V_{zz}, and V_{yy} lie in a plane perpendicular to M1–M1′ in the red mica high in $Fe^{2+}_{M1,M2}$, but in a plane lying between the M1–M2 directions in the two green micas in which the Fe present is predominantly Fe^{3+}. Evidence for Fe^{2+}-Fe^{3+} charge transfer comes from our present and earlier (Finch et al., 1982) polarized absorption measurements and anisotropic magnetic exchange measurements by Ballet and Coey (1982).

The above summary sets out a coherent explanation of the Mössbauer and optical-absorption observations in muscovite single crystals. However, as pointed out in the Introduction, single-crystal Mössbauer measurements in low-symmetry sites are notoriously difficult. Further, if one allows that various different orderings of Fe^{2+} and Fe^{3+} in the M1 and M2 sites, or clustering of ions, may occur, then the problems are multiplied. We have restricted site occupancy to the usually accepted $Fe^{2+}_{M1,M2}$ and Fe^{3+}_{M1}, but one could easily envisage a situation where multiple site occupancy, e.g., by Fe^{3+}, could give rise to highly misleading Mössbauer intensities. Another, seemingly basic, assumption is that crystallographically equivalent, but Mössbauer distinct, M1 or M2 sites are equally populated. If this is not so, then our whole method falls down. Such a situation has apparently been observed by electron paramagnetic resonance for Fe^{3+} in amethyst (Matarrese et al., 1969). If however our interpretation is correct, then there are significant ramifications for Mössbauer studies of other minerals such as clay minerals, amphiboles, and pyroxenes, which also contain Fe^{2+} and Fe^{3+} in edge-sharing octahedra.

Finally, we are mindful of the dangers of neglecting polarization and thickness corrections and the effects on

intensities of anisotropy in the recoil-free fraction, all of which can lead to misleading results (Gibb, 1978). We can only reiterate that our present results are internally self-consistent and indicate that the influence of these factors is small. However, there is an obvious need for further work taking these factors into account. Also it would obviously be meaningful to study muscovites in which only Fe^{2+}_{M1} (e.g., see Ballet and Coey, 1982) or only Fe^{3+}_{M1} (e.g., see Goodman, 1976) is present. The disadvantage is that the usual ambiguities associated with low-symmetry sites remains. Work along these lines, together with theoretical calculations of the EFG (Aldridge et al., 1986, unpub.), is in progress and will be reported subsequently.

ACKNOWLEDGMENTS

REFERENCES

Aldridge, L.P. (1984) AMOSS—A Fortran program for fitting Mössbauer spectra. New Zealand, Department of Scientific and Industrial Research, Report No. C.D.2336.

Annerston, H., and Hålenius, U. (1976) Ion distribution in pink muscovite, a discussion. American Mineralogist, 61, 1045–1050.

Ballet, O., and Coey, J.M.D. (1982) Magnetic properties of sheet silicates; 2:1 layer minerals. Physics and Chemistry of Minerals, 8, 218–229.

Bancroft, G.M. (1973) Mössbauer spectroscopy: An introduction for inorganic chemists and geochemists. Wiley, New York, p. 189.

Bonnin, D., and Muller, S. (1981) Etude du gradient de champ electrique la muscovite par spectrometrie Mössbauer du fer. Physica Status Solidi (b), 105, 649–657.

Chandra, R., and Lokanathan, S. (1977) Electric field gradient in biotite mica. Physica Status Solidi (b), 83, 273–280.

Dyar, M.D., and Burns, R.G. (1986) Mössbauer spectral study of ferruginous one-layer trioctahedral micas. American Mineralogist, 71, 955–965.

Finch, J. (1963) A colorimetric classification of Australian pegmatitic muscovite. American Mineralogist, 48, 525–554.

Finch, J., Gainsford, A.R., and Tennant, W.C. (1982) Polarized optical absorption and ^{57}Fe Mössbauer study of pegmatitic muscovite. American Mineralogist, 67, 59–68.

Gibb, T.C. (1978) The orientation of the electric-field-gradient tensor from single-crystal Mössbauer measurements. Journal of the Chemical Society, Dalton, 743–752.

Goodman, B.A. (1976) The Mössbauer spectrum of a ferrian muscovite and its implications in the assignment of sites in dioctahedral micas. Mineralogical Magazine, 40, 515–517.

Grant, R.W., Housley, R.M., and Gonser, U. (1969) Nuclear electric field gradient and mean square displacement of the iron sites in sodium nitroprusside. Physical Review, 178, 523–530.

Güven, N. (1971) The crystal structures of $2M_1$ phengite and $2M_1$ muscovite. Zeitschrift für Kristallographie, 134, 196–212.

Kemp, R.C. (1972) Electron spin resonance of Fe^{3+} in phlogopite. Journal of Physics C: Solid State Physics, 5, 3566–3572.

——— (1973) Electron spin resonance of Fe^{3+} in muscovite. Physica Status Solidi (b), 57, K79–K81.

McGavin, D.G., and Tennant, W.C. (1985a) Coordinate rotations and the relations amongst the spin-hamiltonian parameters in E.P.R. spectroscopy. Molecular Physics, 55, 853–866.

——— (1985b) EPR study of high-spin ferric ion in a completely rhombic environment. Fe^{3+} in $CaWO_4$. Journal of Magnetic Resonance, 61, 321–332.

Matarrese, L.M., Wells, J.S., and Peterson, R.L. (1969) EPR spectrum of Fe^{3+} in synthetic brown quartz. Journal of Chemical Physics, 50, 2350–2360.

Mombourquette, M.J., Tennant, W.C., and Weil, J.A. (1986) EPR study of Fe^{3+} in α-quartz: A re-examination of the so-called I-centre. Journal of Chemical Physics, 85, 68–79.

Richardson, S.M., and Richardson, J.W. (1982) Crystal structure of a pink muscovite from Archer's Post, Kenya: Implications for reverse pleochroism in dioctahedral micas. American Mineralogist, 67, 69–75.

Townsend, M.G., and Longworth, G. (1985) Sign of the magnetic coupling of Fe^{2+} and Fe^{3+} in biotite. Physics and Chemistry of Minerals, 12, 141–144.

Weil, J.A., Buch, T., and Clapp, J.E. (1973) Crystal point group symmetry and microscopic tensor properties in magnetic resonance spectroscopy. Advances in Magnetic Resonance, 6, 183–257.

Zimmermann, R. (1975) A method for evaluation of single crystal ^{57}Fe Mössbauer spectra ($FeCl_2 \cdot 4H_2O$). Nuclear Instruments and Methods, 128, 537–543.

Zory, P. (1965) Nuclear electric-field gradient determination utilizing the Mössbauer effect (Fe^{57}). Physical Review, 140, A1401–A1407.